77-677

Numerical Calculation of Transonic Potential Flow about Wing-Body Combinations

D. A. Caughey*
Cornell University, Ithaca, N.Y.
and
Antony Jameson†
New York University, New York, N.Y.

A method is presented for numerically calculating the transonic potential flow about rather general geometries. It is based upon a particularly simple form of the usual quasilinear potential equations and is formulated in terms of local representations of the solution and the mapping functions used to generate the finite-difference grid. Thus, all derivatives are generated numerically and there is no need to transform the equation—a formidable task when using boundary-conforming coordinate systems for complex geometries. The solution is stabilized by adding upwind bias in supersonic regions, and the difference equations are solved by relaxation. Sample results for wing-cylinder and simple wing-fuselage combinations are presented.

I. Introduction

THE pioneering numerical solutions of the transonic small-disturbance equation by Murman and Cole[1] and of the complete potential equation for transonic flows by Garabedian and Korn[2] and by Jameson,[3,4] have led to transonic potential solutions for configurations of increasing geometrical complexity. The small-disturbance equation has been solved for lifting, swept wings[5-7] and simple wing-fuselage combinations,[8-12] while the full potential equation has been solved for bodies of revolution,[3,13] axisymmetric and planar inlet nacelles,[14-17] and yawed[4] and swept wings.[18]

One of the major complications of treating the full potential equation rather than its small-disturbance approximation results from the need to treat the boundary conditions accurately. With several exceptions (in which the boundary conditions are satisfied by interpolating on a regular Cartesian mesh[17,19]), this is done by analytically transforming the equation to a boundary-conforming coordinate system so that the boundary conditions can be applied easily (e.g., by reflection) on the body surface itself. This method is particularly attractive when the geometry is relatively simple (e.g., an isolated wing or a semi-infinite inlet nacelle), but the labor involved in transforming the equation (and its attendant chance for error) and the complexity of the finite-difference code grow rapidly with increasing geometrical complexity, so that application of this method to geometries more complicated than a wing-cylinder combination seems unlikely.

An alternative approach is proposed here. It is based upon the particularly simple form the quasilinear potential equation takes under a completely arbitrary coordinate transformation when the velocity is expressed in terms of its contravariant components. The coordinate transformation generating each mesh cell is considered to be independent of the others, and is determined numerically at each step in the calculation from the Cartesian coordinates of the mesh points. For purposes of calculating derivatives, a local trilinear variation of both the independent and dependent variables is assumed, so the method is closely related to a finite-element method using isoparametric elements. The difference equations and artificial viscosity are derived directly from the differential equation, however, not from a variational principle.

A similar analysis has been performed on the conservation form of the continuity equation and is reported in a companion paper.[20] The method is also similar to a scheme used by Rizzi[21] to solve the Euler equations.

Received June 16, 1978; presented as Paper 77-677 at the 10th Fluid and Plasma Dynamics Conference, Albuquerque, N. Mex., June 27-29, 1977; revision received Oct. 13, 1978.

Index categories: Computational Methods; Transonic Flow; Aerodynamics.

*Assistant Professor, Sibley School of Mechanical and Aerospace Engineering. Member AIAA.

†Professor of Computer Science, Courant Institute of Mathematical Sciences. Member AIAA.

II. Analysis

A. Transformation of Potential Equation

Let u,v,w be the velocity components in the x,y,z directions of a Cartesian coordinate system. Then the potential equation is equivalent to the continuity equation

$$\frac{\partial}{\partial x}(\rho u)+\frac{\partial}{\partial y}(\rho v)+\frac{\partial}{\partial z}(\rho w)=0 \tag{1}$$

with derivatives of the density ρ related to the speed of sound a and the magnitude of the velocity q by the energy equation for a calorically perfect gas which gives

$$\frac{\mathrm{d}\rho}{\mathrm{d}q}=-\frac{\rho}{a^2}q$$

and the requirement that the velocity vector be the gradient of some scalar function ϕ. Introducing $Q=\frac{1}{2}q^2$ and multiplying Eq. (1) by a^2/ρ thus gives

$$a^2(u_x+v_y+w_z)-(uQ_x+vQ_y+wQ_z)=0 \tag{2}$$

We next consider an arbitrary (nonsingular) transformation to new independent variables X,Y,Z. We define the Jacobian

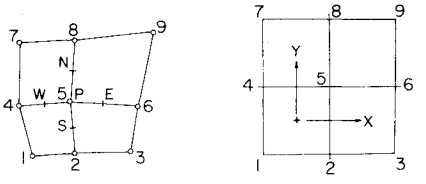

Fig. 1 Geometry of mesh cells.

of this transformation as

$$J=\begin{Bmatrix} x_X & x_Y & x_Z \\ y_X & y_Y & y_Z \\ z_X & z_Y & z_Z \end{Bmatrix} \tag{3}$$

and let $D=\det(J)$. Then, if we define the vector

$$\begin{Bmatrix} U \\ V \\ W \end{Bmatrix} = DJ^{-1} \begin{Bmatrix} u \\ v \\ w \end{Bmatrix} \tag{4}$$

Eq. (2) (after multiplication by D) becomes

$$a^2\{U_X+V_Y+W_Z\}-\{UQ_X+VQ_Y+WQ_Z\}=0 \tag{5}$$

The quantities U, V, and W are the contravariant components of the velocity vector in the new coordinate system, multiplied by D. They are related to the derivatives of the potential in the new coordinate system by

$$\begin{Bmatrix} U \\ V \\ W \end{Bmatrix} = D(J^TJ)^{-1} \begin{Bmatrix} \phi_X \\ \phi_Y \\ \phi_Z \end{Bmatrix} \tag{6}$$

where the matrix J^TJ is the metric tensor of the transformation.

B. Numerical Scheme

The numerical solution of Eq. (5) is based upon its equivalence to the usual quasilinear form of the potential equation, for which reliable numerical schemes have been developed.[4] A finite-difference approximation to the equation is constructed using centered differences everywhere. An explicit artificial viscosity of a form suggested by the "rotated" difference scheme is then added (in conservation form) to the equation at points where the flow is locally supersonic. Finally, an iterative procedure based on an equivalent time-dependent process is constructed to solve the resulting difference equations.

The basic central-difference approximation to Eq. (5) can be visualized in two dimensions by considering the solution in the vicinity of the common point P of four neighboring mesh cells as in Fig. 1. (The analogous three-dimensional formulas follow from a straightforward extension of this geometry to include the eight neighboring cells.) In each mesh cell we consider the physical coordinates and the velocity potential to be represented by a local bilinear mapping. Thus, in cell 1-2-5-4, for example,

$$x=\tfrac{1}{4}\{x_1(1-X)(1-Y)+x_2(1+X)(1-Y) +x_4(1-X)(1+Y)+x_5(1+X)(1+Y)\} \tag{7}$$

where X and Y are local coordinates centered in the cell whose vertices lie at (1,1), (−1,1), (1,−1), and (−1,−1). Similar formulas hold for y and z, and

$$\phi=\tfrac{1}{4}\{\phi_1(1-X)(1-Y)+\phi_2(1+X)(1-Y) +\phi_4(1-X)(1+Y)+\phi_5(1+X)(1+Y)\} \tag{8}$$

Thus, at the points N, E, S, and W we can calculate, consistent with this local approximation, quantities such as (e.g., at E)

$$x_X=\tfrac{1}{2}(x_6-x_5) \tag{9}$$

and

$$x_Y=\tfrac{1}{8}(x_8-x_2+x_9-x_3)$$
$$\phi_Y=\tfrac{1}{8}(\phi_8-\phi_2+\phi_9-\phi_3) \tag{10}$$

Note that in this approximation derivatives along a cell boundary are continuous across the boundary, but derivatives normal to the boundary are not, requiring the use of suitable averages as in Eqs. (10). In this manner, numerical approximations to the Jacobian matrix and potential derivatives are obtained, and can be used to calculate the velocity components U and V according to Eq. (6). In practice, it is convenient to introduce a reduced velocity potential G by subtracting out the contribution due to a freestream at angle of attack α

$$\phi=G+x\cos\alpha+y\sin\alpha \tag{11}$$

and first determine the Cartesian velocity components by

$$\begin{Bmatrix} u \\ v \end{Bmatrix} = \begin{Bmatrix} \cos\alpha \\ \sin\alpha \end{Bmatrix} + (J^{-1})^T \begin{Bmatrix} G_X \\ G_Y \end{Bmatrix} \tag{12}$$

Then

$$\begin{Bmatrix} U \\ V \end{Bmatrix} = DJ^{-1} \begin{Bmatrix} u \\ v \end{Bmatrix} \tag{13}$$

and

$$Q=\tfrac{1}{2}(u^2+v^2) \tag{14}$$

Once the velocities are determined at the points N, E, S, and W, the equation at P is approximated by

$$a^2\{U_E-U_W+V_N-V_S\}-\{U(Q_E-Q_W)+V(Q_N-Q_S)\}=0 \tag{15}$$

with a^2 determined by the energy equation to be

$$a^2=a_0^2-(\gamma-1)Q \tag{16}$$

where a_0 is the stagnation speed of sound.

The centered-difference approximation just described is unstable in supersonic regions because all of the operators are symmetric with respect to a reversal of the sign of the velocity vector. To stabilize the solution in supersonic zones, it is necessary to add a directional bias to the equations, which can be done by incorporating a suitable numerical, or artificial, viscosity. If s is taken to be a coordinate in the direction of the local velocity vector, then Eq. (5) is equivalent to

$$D\{(a^2-q^2)\phi_{ss}+a^2(\nabla^2\phi-\phi_{ss})\}=0 \tag{17}$$

In terms of the computational variables,

$$\phi_s=(1/Dq)\{U\phi_X+V\phi_Y+W\phi_Z\} \tag{18}$$

so the principal part of ϕ_{ss} is

$$\phi_{ss}=(1/D^2q^2)\{U^2\phi_{XX}+V^2\phi_{YY}+W^2\phi_{ZZ} +2UV\phi_{XY}+2UW\phi_{XZ}+2VW\phi_{YZ}\} \tag{19}$$

A directional bias is incorporated into the equation by adding terms equivalent to those introduced by evaluating ϕ_{ss} in the first term of Eq. (17) using upwind differences in Eq. (19). This is equivalent to rewriting Eq. (5) as

$$a^2\{U_X+V_Y+W_Z\}-\{UQ_X+VQ_Y+WQ_Z\} +\{f_X+g_Y+h_Z\}=0 \tag{20}$$

with (for U, V, and W all positive)

$$f=(\mu/D)\Delta X\{U^2\phi_{XX}+2UV\phi_{XY}+2UW\phi_{XZ}\} \quad (21a)$$

$$g=(\mu/D)\Delta Y\{2UV\phi_{XY}+V^2\phi_{YY}+2VW\phi_{YZ}\} \quad (21b)$$

$$h=(\mu/D)\Delta Z\{2UW\phi_{XZ}+2VW\phi_{YZ}+W^2\phi_{ZZ}\} \quad (21c)$$

where μ is the switching function defined by

$$\mu=\max(1-a^2/q^2,\ 0) \quad (22)$$

If U, V, or W is negative, Eqs. (21) are modified to reflect the appropriate upwind differencing. This scheme corresponds to a quasiconservative form of Jameson's rotated differencing scheme[22,23]; that is, although the equation is differenced in its quasilinear (nonconservation) form, the artificial viscosity is added in conservation form.

The difference equations resulting from this procedure are highly implicit, so a relaxation solution of them necessarily introduces mixed space and time derivatives (if the iteration steps are considered increments in an artificial time). Our iterative scheme is modelled after a stable scheme devised by Jameson for the equations resulting from the rotated difference scheme applied to the usual quasilinear equation.[4,24] Let i, j, and k represent the indices of the mesh points in the X, Y, and Z directions, respectively. Then if U, V, and W are all positive, the correction $C_{i,j,k}$ to be added to the reduced potential at each point is determined by solving (e.g., for a successive line scheme in the direction of the j index)

$$\alpha_1(C_{i,j,k}-C_{i,j-1,k})+\alpha_2(C_{i,j,k}-C_{i,j+1,k})+\alpha_3(C_{i,j,k}-C_{i-1,j,k})$$
$$+\alpha_4(C_{i,j,k}-C_{i,j,k-1})+\alpha_5 C_{i,j,k}=4R \quad (23)$$

where R is the residual of Eq. (20), evaluated with values of the potential from the previous iteration. The coefficients are given by

$$\alpha_1=Da^2B_{22}-V^2/D+3(\mu/D)V^2+2\omega_s V(U+V+W)/Dq^2$$

$$\alpha_2=Da^2B_{22}-V^2/D+(\mu/D)V^2$$

$$\alpha_3=Da^2B_{11}-U^2/D+3(\mu/D)U^2+2\omega_s U(U+V+W)/Dq^2$$

$$\alpha_4=Da^2B_{33}-W^2/D+3(\mu/D)W^2+2\omega_s W(U+V+W)/D_q^2$$

$$\alpha_5=[(2/\omega_r)-1](Da^2(B_{11}+B_{33})-(U^2+W^2)/D) \quad (24)$$

where B_{11}, B_{22}, and B_{33} are the diagonal elements of the matrix $(J^TJ)^{-1}$. Again, if U, V, or W is negative, Eqs. (23) and (24) must be appropriately modified. The parameters ω_r and ω_s govern the stability and convergence rate in the subsonic and supersonic regions, respectively. The subsonic overrelaxation factor ω_r is chosen between 1 and 2, with fastest convergence requiring a value approaching 2 as the mesh spacing goes to zero. The ω_s factor governs the amount of additional ϕ_{st} term added to the equivalent time dependent equation governing the relaxation process; larger values lead to a more stable iteration but slower convergence.

C. Treatment of Geometry

One advantage of a method that requires only a local description of the mapping function is that it essentially decouples the solution process from the generation of the grid network. That is, the finite-difference grid can be constructed in any convenient manner, and all that is subsequently required are the Cartesian coordinates of the mesh points. One method for generating the computational grid is to use an analytical transformation based upon a sequence of simple conformal and shearing transformations, which reduces the geometry to a convenient domain. This method has been used

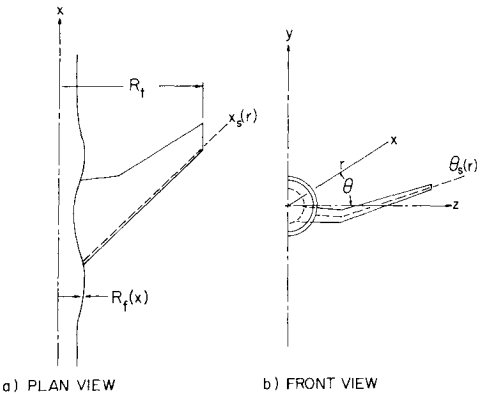

Fig. 2 Wing-fuselage configuration.

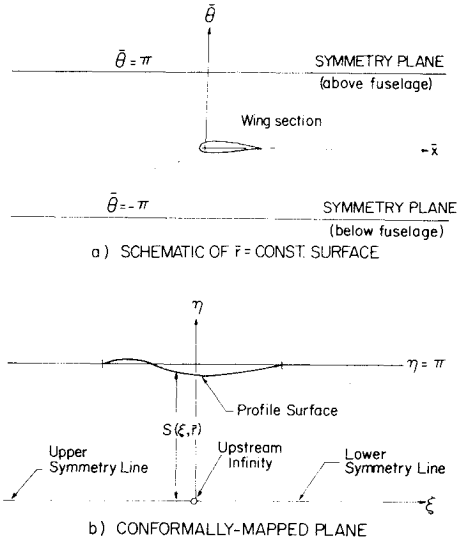

Fig. 3 Schematic of conformal mapping.

in earlier work (for simpler geometries) that took advantage of the analytical nature of the transformations and solved the transformed equation in the new computational domain. When the geometry is sufficiently complex, however, transformation of the equation under the required sequence of mappings becomes extremely tedious, and the number of terms in the final equation so large that the alternative method presented here becomes attractive not only from an algebraic point of view, but from a computational one as well. The generation of the grid using these transformations is still an attractive idea, however, since the resulting network is smoothly-varying, in many cases nearly orthogonal, and boundary-conforming. And, of course, the computational labor involved in determining the coordinates of the grid points is far less than that required to transform the equation.

The geometry chosen as a test for these ideas is shown in Fig. 2. It consists of a wing of arbitrary planform and dihedral mounted on a fuselage of circular cross section. The fuselage radius is allowed to change in the axial direction, but must approach a constant nonzero value at upstream and downstream infinity. The geometry is first normalized by the transformation

$$\bar{x}=\frac{x-x_s(\bar{r})}{c(\bar{r})}+\log 2 \quad (25a)$$

$$\bar{r}=\frac{r-R_f(x)}{R_t-R_f(x)} \quad (25b)$$

$$\bar{\theta}=2\left[\theta-\frac{(1-(4/\pi^2)\theta^2)}{1-(4/\pi^2)\theta_s^2(\bar{r})}\theta_s(\bar{r})\right] \quad (25c)$$

where $R_f(x)$ and R_t are the fuselage radius and wing-tip radius (assumed constant), respectively, $c(\bar{r})$ is the local wing chord; and $x_s(\bar{r})$ and $\theta_s(\bar{r})$ are the coordinates of a line just inside the wing leading-edge, about which the profile will be subsequently "unwrapped" in surfaces of constant $\bar{r}$. In these surfaces, the geometry looks like that shown in Fig. 3a. The transformation

$$\bar{x}+i\bar{\theta}=\log\{1-\cosh(\xi+i\eta)\} \tag{26}$$

maps these surfaces to the geometry of Fig. 3b. The width of the strip $S(\xi,\bar{r})$ is a slowly-varying function of ξ if the location of the singular line has been carefully chosen. Finally, the transformation

$$X=\xi, \quad Y=\eta/S(\xi,\bar{r}), \quad Z=\bar{r} \tag{27}$$

and suitable stretching transformations in the X and Z directions reduce the geometry to the finite rectangular box shown in Fig. 4. Since the present method evaluates all derivatives numerically, the computational domain must be truncated at some finite distance from the body, so the final domain corresponds to a rectangular box slightly shorter in the $\pm X$ and Z directions and with the neighborhood of the upstream infinity line at $X=0$, $Y=0$ excluded. A uniform rectangular mesh in this domain is then mapped back to the physical domain to give the Cartesian coordinates of the grid points.

One final word should be said about the stretching functions used in the mapping to the final computational domain. Since Y is essentially an angular coordinate, a uniform grid spacing leads to poor resolution near the wing tip, where the cells become highly elongated in the vertical direction. To avoid this problem, a stretching function was introduced which packs lines of constant Y nearer the wing surface as Z increases, in a manner that results in nearly constant cell height in the vicinity of the plane of the wing. It should be noted that the introduction of such a multivariable stretching would greatly complicate transformation of the potential equation, if this were required. In the present method, however, it is a minor change, accomplished with two or three FORTRAN statements in the subroutine which constructs the grid.

The incorporation of the boundary conditions into the solution procedure in such a boundary-conforming coordinate system is particularly simple when the potential equation is cast in the form of Eq. (5). Since U, V, and W are proportional to the contravariant components of the velocity vector, and hence to the velocities normal to the coordinate surfaces, the boundary conditions simply require that component that does not lie in the boundary surface to be zero. Thus, referring to Fig. 4, the appropriate fuselage boundary condition is $W=0$, whereas on the wing surface and symmetry plane we require $V=0$. These boundary conditions are incorporated directly into the equation at boundary points, with one-sided differences used to evaluate the necessary potential and mapping derivatives there.

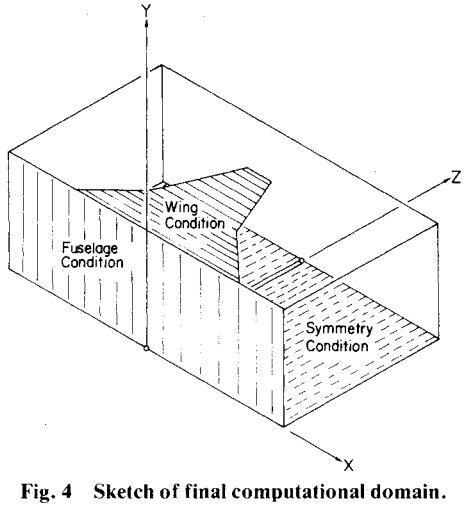

Fig. 4 Sketch of final computational domain.

A further complication is introduced by the presence of a vortex sheet downstream of the wing trailing edge when the wing has lift. The true vortex sheet is a contact discontinuity across which the tangential velocity components are discontinuous, and which experiences convection as well as self-induced roll-up. We neglect the rolling up of the sheet and approximate its convection by assuming that its location is represented by a continuation of the branch cut in Fig. 3a which leaves the trailing edge smoothly and returns to the plane of the wing at downstream infinity. On this surface, we require

$$V_Y=0 \tag{28}$$

since the normal velocity component is continuous at the sheet. A constant discontinuity in the potential is assumed in each spanwise surface, its value determined by the Kutta condition at the trailing edge.

In order for the relaxation scheme described in the preceding section to be stable, the direction in which the field is swept must not oppose the velocity vector in any supersonic zone. For the geometries we consider, this is insured by sequentially solving the Z planes, starting with the fuselage and proceeding outboard to the far-field boundary. In each Z plane, the sweep direction corresponds to the sign of X; that is, lines intersecting the wing lower surface are swept to the right in the computational domain, and those intersecting the upper surface are swept to the left (see Fig. 3). This procedure has proved adequate even when the freestream Mach number is supersonic; i.e., when the local Mach number at virtually all the field points is supersonic.

III. Results

A. Computational Considerations

The calculation of three-dimensional transonic potential flows about realistic wing-fuselage geometries is a task which exercises the capabilities of current computers to their limits. Thus, at this point, a few words about the logical layout of the computer program might be in order. The storage of the solution array and the Cartesian coordinates of each mesh point for the grids used here (containing 122,880 cells) would require about 1700 K (octal) on a CDC machine, or about 1900 K (decimal) on an IBM machine. Clearly it is not practical to store these arrays in high-speed core, nor is it necessary, since only a small part of these arrays is being operated upon at any given instant. Since the relaxation solution naturally proceeds from one $Z=$ constant plane to the next, it is necessary to have available in high-speed core only the coordinates and solution array for the current plane and its neighbor to either side, plus the "old" values of the solution on the preceding plane. Thus, the complete arrays are stored on, say, a disk, and sequentially buffered in and out of core as needed. This buffering is most efficiently performed asynchronously while the computations are in progress, so an additional array for each of the quantities is used for this purpose. To avoid recalculating W, Q, and h on the $(k-\frac{1}{2})$ plane (which is the $(k+\frac{1}{2})$ plane for the preceding plane), these quantities are also stored, bringing the total required to some 20 two-dimensional arrays (of 4347 values each, including the dummy points associated with boundaries). The complete program, dimensioned for these values, requires 142 K SCM and 200 K LCM on the CDC 7600.

The relaxation part of the program is constructed so that the same difference equations are used at all points, including boundary points. This is achieved by introducing dummy

values at points "behind" each boundary, with values set such that the difference equations produce the same results as the appropriate one-sided formulas. Also, the appropriate quantities from the preceding line or point entering into the X and Y differences at each point are also stored, so that only three (of the six) velocities need be calculated at each point.

Finally, since the convergence rate of the iterative process decreases as the mesh spacing goes to zero, it is effective to perform a sequence of calculations, starting with a crude grid and successively refining it, using the previous solution as a starting guess at each step of the procedure. A single relaxation sweep of the entire field requires about 17 s for the 122,880-cell mesh, so a solution consisting of 100 relaxation cycles on each of two preliminary grids containing 1920 and 15,360 cells, respectively, followed by 50 cycles on the final grid, requires less than 19 min of CPU time on the CDC 7600.

B. Sample Computations

In this section we present the results of several preliminary calculations to demonstrate the capabilities of the method we have described. All the results presented have been calculated on a grid containing $160 \times 24 \times 32$ mesh cells in the X, Y, and Z directions, respectively, corresponding to the computing resources described in the preceding section. It is emphasized that these results are preliminary, as no attempt has been made to systematically optimize the grid. It is, of course, an advantage of the finite volume approach that alternative grid networks can be easily incorporated and tested.

The first solution is for the ONERA Wing M-6, mounted on a cylindrical fuselage having a radius of 0.25 times the exposed semispan, as shown in Fig. 5. The details of the wing geometry are given in Ref. 25, and a number of comparisons with experimental data for the wall-mounted wing are given in Ref. 18. The calculation shown here is for an angle of attack (of the wing and fuselage) of 3.06 deg and a Mach number of 0.840. Comparisons of the streamwise pressure distributions calculated using the present method with those of a fully-conservative scheme[20] are shown at four spanwise stations in Fig. 6. The agreement is good, including shock strengths and positions. The ability of the present quasiconservative scheme to reproduce the shock jump of the full conservation scheme is particularly striking at the 94% semispan station.

The second sequence of calculations presents results illustrating the ability of the method to model fuselage geometry effects at both subsonic and supersonic freestream Mach numbers. The calcualtions are for the flow about two wing-body configurations tested experimentally by McDevitt.[26] Both configurations utilize the same wing. It is a symmetric, uniformly tapered wing defined by the NACA

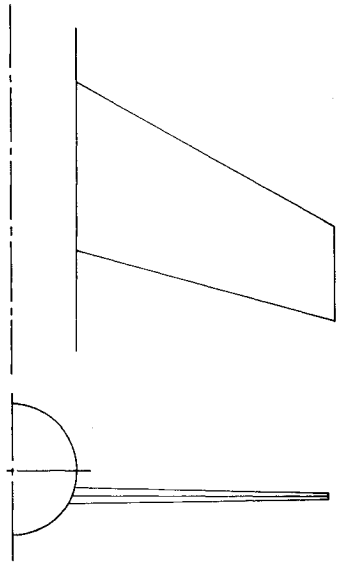

Fig. 5 ONERA wing M-6 on cylindrical fuselage.

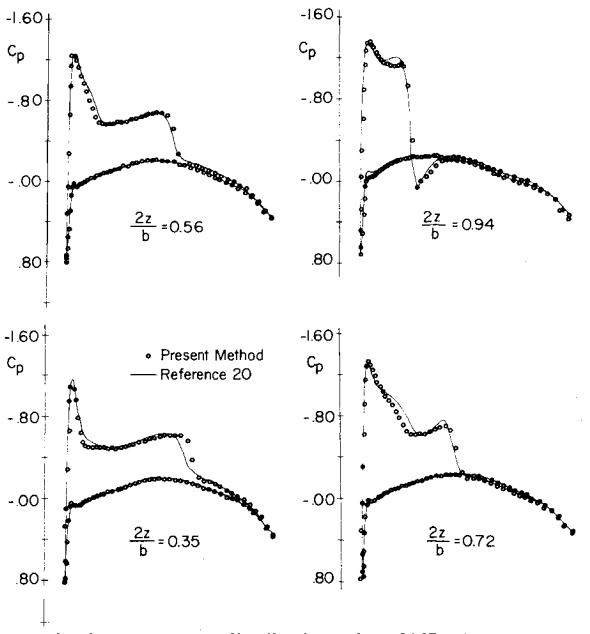

Fig. 6 Surface pressure distributions for ONERA wing-cylinder combination at $M_\infty = 0.84$ and $\alpha = 3.06$ deg.

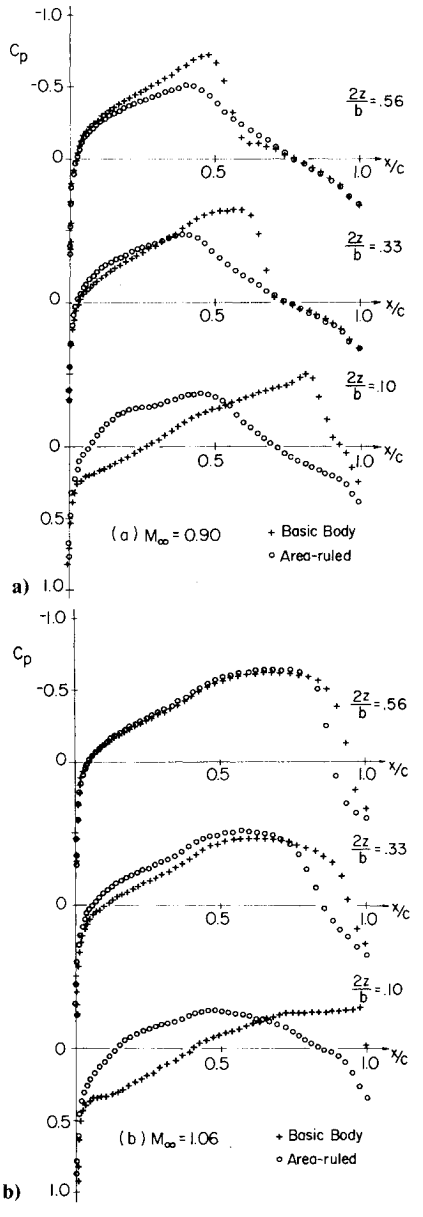

Fig. 7 Effect of fuselage area ruling on wing surface pressure distributions for NACA configurations.[26]

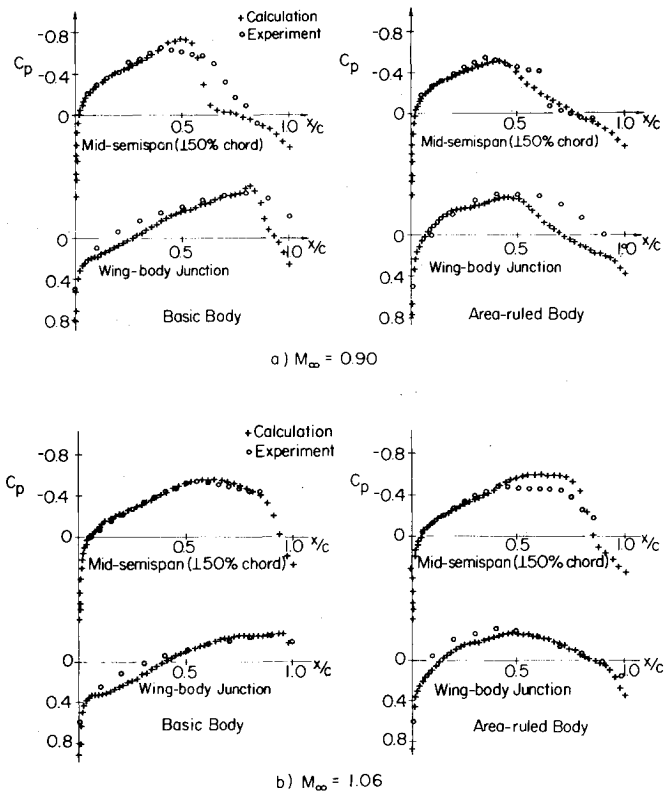

Fig. 8 Comparison with experimental pressure distributions for NACA configurations.[26]

64_2A015 section in planes normal to the midchord line. The midchord line is swept back at 35 deg, and the wing has an aspect ratio of 6.0. In the first configuration, herein called the "basic body," the wing is mid-mounted on an axisymmetric fuselage having a maximum radius equal to one eighth the semispan and a cross-sectional area distribution corresponding to a Sears-Haack body of fineness ratio nine. In the second configuration, called the "area-ruled body" here, the basic body is modified for wing volume according to the Mach 1 area rule, then increased in scale until the original enclosed fuselage volume is recovered. A detailed model description is contained in Ref. 26. For our calculations both bodies were modified to include cylindrical forebodies extending upstream to infinity, having cross-sectional areas of 5% of the fuselage maxima. The experimental mounting stings were assumed to extend to downstream infinity. All calculations were performed at 0-deg angle of attack, since this was the only condition for which experimental pressure distributions were available.

The first set of results illustrates the effect on the wing pressure distribution of the fuselage area ruling. Figures 7a and b present the wing pressure distributions at three nearly-streamwise stations for Mach numbers of 0.90 and 1.06, respectively. The three stations correspond to intersections of the wing with grid surfaces, and are not quite vertical planes because of the way in which the coordinates are generated; the innermost station ($2z/b = 0.10$) corresponds to the wing-body junction. As can be seen from the figures, the shock strength is greatly reduced by the area ruling, especially inboard. Also, the isobars are more nearly parallel in the area ruled case; this effect is particularly noticeable in the $M = 0.90$ case, where the pressure distibutions outboard of the 33% semispan are nearly identical.

The next set of results compares the calculated pressure distributions with those measured by McDevitt[26] at the wing-body junction and at the mid-semispan, normal to the 50% chord line. (For these latter comparisons, interpolation of the computed results was necessary.) Figures 8a and b present

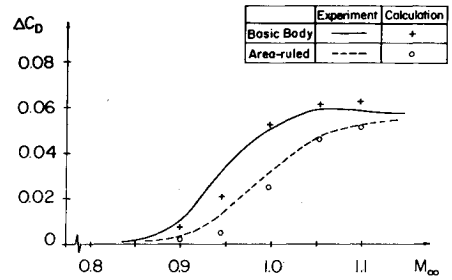

Fig. 9 Predicted and measured drag-rise characteristics of NACA configurations at zero lift.

these comparisons, again at freestream Mach numbers of 0.90 and 1.06, respectively. As can be seen, agreement is quite good except in the vicinity of the shock, when it is appreciably upstream of the trailing edge, and in regions of adverse pressure gradient at the wing-body juncture; in both these cases, viscous effects, which are not modelled here, are certainly important.

Finally, results for the zero-lift drag rise through Mach 1 for the two configurations are presented in Fig. 9. The calculated values were determined from surface-pressure integrations over the entire configuration; the values of the drag coefficient at $M_\infty = 0.80$ were subtracted from the experimentally obtained results. The calculated and measured results are in rather remarkable agreement, with the trends due to fuselage geometry well predicted as well as the absolute values.

IV. Conclusions

A method has been presented for calculating transonic solutions to the full potential equation about rather general three-dimensional bodies. The method is illustrated for a class of wing-body combinations for which a boundary-conforming finite-difference grid can be generated easily using a sequence of shearing transformations and an analytical conformal mapping. The numerical method is not limited to this particular mesh generation scheme, and others, e.g., that used in Ref. 20, should be investigated for the wing-body problem.

A second area that warrants further study is that of convergence acceleration of the iterative scheme. Three-dimensional solutions are, by their nature, very costly in terms of computer time, and the potential for savings is great if the number of iterations required can be substantially reduced. Several approaches have been suggested for simpler problems[15,27-30] and should be investigated in the context of three-dimensional transonic calculations.

Acknowledgment

This work was supported by the Office of Naval Research under Contract N00014-77-C-0033. Some of the calculations were performed at the ERDA Mathematics and Computing Laboratory, New York University, under Contract E(11-1)-3077.

References

[1] Murman, E. M. and Cole, J. D., "Calculation of Plane, Steady, Transonic Flows," *AIAA Journal*, Vol. 9, Jan. 1971, pp. 114-121.

[2] Garabedian, P. R. and Korn, D. G., "Analysis of Transonic Airfoils," *Comm. Pure Appl. Math.*, Vol. 24, 1971, pp. 841-851.

[3] Jameson, A., "Transonic Flow Calculations for Airfoils and Bodies of Revolution," Grumman Aerodynamics Report 370-71-1, 1971.

[4] Jameson, A., "Iterative Solution of Transonic Flows over Airfoils and Wings, Including Flows at Mach 1," *Comm. Pure Appl. Math.*, Vol. 27, 1974, pp. 283-309.

[5] Ballhaus, W. F. and Bailey, F. R., "Numerical Calculation of Transonic Flow about Swept Wings," AIAA Paper 72-677, Boston, Mass., June 1972.

[6] Lock, R. C., "Research in the U.K. on Finite-Difference Methods for Computing Steady, Transonic Flows," *Symposium Transsonicum II*, Springer-Verlag, New York, 1976, pp. 457-486.

[7] vander Vooren, J., Sloof, J. W., Huizing, G. H., and van Essen, A., "Remarks on the Suitability of Various Transonic Small Perturbation Equations to Describe Three-Dimensional Transonic Flow; Examples of Computations using a Fully-Conservative Rotated Difference Scheme," *Symposium Transsonicum II*, Springer-Verlag, New York, 1976, pp. 557-566.

[8] Bailey, F. R. and Ballhaus, W. F., "Relaxation Methods for Transonic Flow about Wing-Cylinder Combinations and Lifting, Swept Wings," *Lecture Notes in Physics*, Vol. 19, Springer-Verlag, New York, 1972, pp. 2-9.

[9] Newman, P. A. and Klunker, E. B., "Numerical Modeling of Tunnel-Wall and Body-Shape Effects on Transonic Flow Over Finite, Lifting Wings," NASA SP-347, part II, 1975, pp. 1189-1212.

[10] Bailey, F. R. and Ballhaus, W. F., "Comparisons of Computed and Experimental Pressures for Transonic Flows about Isolated Wings and Wing-Fuselage Configurations," NASA SP-347, Pt. II, 1975, pp. 1213-1231.

[11] Schmidt, W. and Vanino, R., "The Analysis of Arbitrary Wingbody Combinations in Transonic Flow using a Relaxation Method," *Symposium Transsonicum II*, Springer-Verlag, New York, 1976, pp. 523-532.

[12] Albone, C. M., Hall, M. G., and Joyce, G., "Numerical Solution for Transonic Flows Past Wing-Body Combinations," *Symposium Transsonicum II*, Springer-Verlag, New York, 1976, pp. 541-548.

[13] South, J. C., Jr., and Jameson, A., "Relaxation Solutions for Inviscid Axisymmetric Transonic Flow over Blunt or Pointed Bodies," *Proceedings of AIAA Computational Fluid Dynamics Conference*, Palm Springs, Calif., July 1973, pp. 8-17.

[14] Arlinger, B. G., "Calculation of Transonic Flow around Axisymmetric Inlets," AIAA Paper 75-80, Pasadena, Calif., Jan. 1975; also *AIAA Journal*, Vol. 13, Dec. 1975, pp. 1614-1621.

[15] Caughey, D. A. and Jameson, A., "Accelerated Iterative Calculation of Transonic Nacelle Flowfields," *AIAA Journal*, Vol. 15, Oct. 1977, pp. 1474-1480.

[16] Baker, T. J., "A Numerical Method to Compute Inviscid Transonic Flows about Axisymmetric Ducted Bodies," *Symposium Transsonicum II*, Springer-Verlag, New York, 1975, pp. 495-506.

[17] Reyhner, T. A., "Cartesian Mesh Solution for Axisymmetric Transonic Potential Flow around Inlets," AIAA Paper 76-421, San Diego, Calif., June, 1976; also *AIAA Journal*, Vol. 15, May 1977, pp. 624-631.

[18] Jameson, A. and Caughey, D. A., "Numerical Calculation of the Transonic Flow past a Swept Wing," New York Univ. ERDA Rept. C00 3077-140, May 1977.

[19] Carlson, L. A., "Transonic Airfoil Analysis and Design using Cartesian Coordinates," *Proceedings of AIAA 2nd Computational Fluid Dynamics Conference*, Hartford, Conn., June 19-20, 1975, pp. 175-183.

[20] Jameson, A. and Caughey, D. A., "A Finite-Volume Method for Transonic Potential Flow Calculations," *Proceedings of AIAA 3rd Computational Fluid Dynamics Conference*, Albuquerque, N. Mex., June 27-28, 1977, pp. 35-54.

[21] Rizzi, A., "Transonic Solutions of the Euler Equations by the Finite Volume Method," *Symposium Transsonicum II*, Springer-Verlag, New York, 1976, pp. 567-574.

[22] Bauer, F. and Korn, D., "Computer Simulation of Transonic Flow past Airfoils with Boundary Layer Correction," *Proceedings of AIAA 2nd Computational Fluid Dynamics Conference*, Hartford, Conn., June 19-20, 1975, pp. 184-204.

[23] Bauer, F., Garabedian, P., Korn, D., and Jameson, A., *Supercritical Wing Sections II*, Springer-Verlag, New York, 1975.

[24] Jameson, A., "Transonic Potential Flow Calculations using Conservation Form," *Proceedings of AIAA 2nd Computational Fluid Dynamics Conference*, Hartford, Conn., June 1975, pp. 148-161.

[25] Monnerie, B. and Charpin, F., "Essais de buffeting d'une aile en flèche en transsonique," 10e Colloque d'Aerodynamique Appliqué, Lille, France, Nov. 1973.

[26] McDevitt, J. B., "An Experimental Investigation of Two Methods for Reducing Transonic Drag of Swept-Wing and Body Combinations," NACA RM A55B21, 1955.

[27] Jameson, A., "Accelerated Iteration Schemes for Transonic Flow Calculations using Fast Poisson Solvers," New York Univ. ERDA Rept. C00-3077-82, 1975.

[28] Jameson, A., "An Alternating Direction Method for the Solution of the Transonic Small-Disturbance Equations," New York Univ. ERDA Rept. C00-3077-96, 1975.

[29] Hafez, M. M. and Cheng, H. K., "Convergence Acceleration and Shock Fitting for Transonic Flow Computations," AIAA Paper 75-51, Pasadena, Calif., Jan. 1975.

[30] South, J. C. and Brandt, A., "Application of the Multi-Level Grid Method to Transonic Flows," Project SQUID Workshop on Transonic Flow Problems in Turbomachinery, Monterey, Calif., Feb. 1976.